Low energy deuteron-induced reactions on Fe isotopes

M. Avrigeanu,[1,*] V. Avrigeanu,[1] P. Bém,[2] U. Fischer,[3] M. Honusek,[2] K. Katovsky,[4] C. Mănăilescu,[1] J. Mrázek,[2] E. Šimečková,[2,†] and L. Závorka[2]

[1]*Horia Hulubei National Institute for Physics and Nuclear Engineering, P.O. Box MG-6, 077125 Bucharest-Magurele, Romania*

[2]*Euratom/IPP.CR Fusion Association, Nuclear Physics Institute, 25068 Řež, Czech Republic*

[3]*Euratom/FZK Fusion Association, Karlsruhe Institute of Technology (KIT), Hermann-von-Helmholtz-Platz 1, 76344 Eggenstein-Leopoldshafen, Germany*

[4]*Czech Technical University, V Holešovičkách 2, 180 00 Prague, Czech Republic*

(Received 28 March 2014; published 24 April 2014)

The activation cross sections for production of ^{51}Cr, ^{52,54,56}Mn, ^{59}Fe, and ^{55,56,57,58}Co radioisotopes in deuteron-induced reactions on natural Fe were measured at deuteron energies up to 20 MeV. Then, within an extended analysis of deuteron interactions with ^{nat}Fe, all processes from elastic scattering until the evaporation from fully equilibrated compound system have been taken into account. Following the available elastic-scattering data analysis that supports the deuteron optical potential for reaction cross sections calculations, increased attention is paid especially to the breakup (BU) mechanism and direct reactions (DR). The deuteron activation cross-section analysis is completed by consideration of the preequilibrium and compound-nucleus contributions, corrected for decrease of the total reaction cross section due to the leakage of the initial deuteron flux towards BU and DR processes. The overall agreement of the measured data and model calculations validates the description of nuclear mechanisms taken into account, particularly the strong effects of direct interactions that have still not been appropriately considered within previous deuteron activation evaluations.

DOI: 10.1103/PhysRevC.89.044613 PACS number(s): 24.10.Eq, 24.10.Ht, 25.45.De

I. INTRODUCTION

The present work continues the series of recent deuteron-induced reaction data analyses, looking for a consistent way to include also the breakup contribution within the activation cross-section calculations [1–6]. Such analyses should meet the demands of several on-going strategic research programs at international large-scale facilities [7–9] that involve deuteron beams and are focused on both academic research and applied physics related to neutron as well as deuteron-induced reactions [10].

The description of deuteron-nucleus interaction represents actually an important test of the reaction mechanism models. The deuteron weak binding energy of 2.224 MeV is responsible for the high complexity of the interaction process that supplementally involves a variety of reactions initiated by the neutrons and protons following the deuteron breakup (BU). This has been the main reason hampering so far a comprehensive analysis involving large mass range of target nuclei and incident-energy domain. On the other hand, the open questions on this topic began with the key ingredient for any calculation of deuteron activation cross sections; that is, the deuteron optical model potential (OMP). The very few measurements of deuteron elastic scattering angular distributions as well as of total reaction cross section corresponding to a specific target nucleus made the assessment of a deuteron OMP difficult. Consequently, a simultaneous comparative analysis of the experimental deuteron elastic-scattering and total reaction cross sections, and the corresponding predictions of various deuteron global OMPs, is critical for an accurate assessment of the most appropriate potential. Next, the (d,p) and (d,n) stripping as well as the (d,t) and (d,α) pick-up direct reaction (DR) contributions have been shown to be important at low incident energies [11–16]. Consequently, an appropriate treatment within the coupled-reaction channels (CRC) formalism was required and used. Thus, the present work concerns a deeper understanding of deuteron breakup, stripping, and pick-up reactions, all together and consistently with the better known statistical emission within the preequilibrium (PE) and compound-nucleus (CN) processes.

The experimental setup and the measured data are described in Sec. II. Next, a consistent energy-dependent optical potential for deuterons on Fe isotopes is discussed in Sec. III A. Deuteron breakup effects on the corresponding activation data of Fe isotopes are established in Sec. III B, while the DR analysis using the computer code FRESCO [17] is described in Sec. III C, and that of PE and CN contributions, using the code TALYS-1.4 [18], is discussed in Sec. III D. The measured and calculated deuteron activation cross sections of Fe isotopes and natural element are discussed in Sec. IV, including the evaluated data from the TENDL-2013 library [19], and conclusions of this work are given in Sec. V. Partial and preliminary results were presented elsewhere [20–22].

II. MEASUREMENTS

The irradiation was carried out using an external deuteron beam of the NPI variable-energy cyclotron U-120M operating in the negative-ion mode of acceleration. From the stripping-foil extractor the beam was delivered to the reaction chamber through a beam line consisting of one dipole and two quadrupole magnets. The energy was determined with

*marilena.avrigeanu@nipne.ro
†simecek@ujf.cas.cz

TABLE I. Characteristics of single runs.

Run no.	Initial energy (MeV)	Total charge (μC)	Irradiation time (s)	Mean current (μA)
1	20.02	362.0	1820	0.199
2	20.05	405.0	1667	0.243

a resulting accuracy of 1%, and the FWHM spread of the incident beam up to 1.8% was observed.

The activation cross sections were measured by the stacked-foil technique. The collimated deuteron beam strikes the stack of foils in a Faraday-cup-like reaction chamber, enabling us to employ the cooling of stacked foils without the loss of accuracy in the beam current and charge monitoring ($\sim$5%).

The high purity Fe foils (Goodfellow product, 99.9% purity, 25 μm declared thickness) and Al (50 μm declared thickness) were weighed (within 2% of accuracy) to avoid relatively large uncertainties in the foil thickness declared by the producer. The mean energy, energy thickness, and energy spread in each foil were set out by SRIM 2008 code [23]. The foils of the examined element Fe were inserted in the chamber alternately with Al foils that were used for additional monitoring of the beam current and appropriate reduction of the deuteron energy as well.

Natural iron consists of four stable isotopes: ^{54}Fe (5.8%), ^{56}Fe (91.72%), ^{57}Fe (2.2%), and ^{58}Fe (0.28%) which leads to many channels opening. The irradiation was carried through two runs to check the internal consistency of the measurement. The characteristics of the single runs are given in Table I.

The gamma rays from the irradiated foils were measured repeatedly by a calibrated high-purity germanium (HPGe) detector of 50% efficiency and FWHM of 1.8 keV at 1.3 MeV. Experimental reaction rates were calculated from the specific activities at the end of the irradiation and corrected to the decay during irradiation using total charge and foil characteristics as well. The measurement with different cooling times lasted up to 100 days after irradiation. The decay data of the isotopes observed from irradiated Fe foils [24] are given in Table II.

TABLE II. Half-lives, main gamma lines, and their intensities [24] of the isotopes observed from irradiated Fe foils.

Isotope	$T_{1/2}$	E_γ (keV)	I_γ (%)
^{51}Cr	27.703 d	320.082	10
^{52}Mn^m	21.1 m	1434.068	98.3
		377.748	1.7
^{52}Mn	5.591 d	1434.068	100
		935.538	94.5
		744.233	90.0
^{54}Mn	312.3 d	834.848	99.98
^{56}Mn	2.579 h	846.771	98.9
		1810.772	27.2
^{59}Fe	44.503 d	1099.251	56.5
		1291.595	43.2
^{55}Co	17.53 h	931.3	75
		477.2	20.2
^{56}Co	77.27 d	846.771	100
		1771.35	15.69
^{57}Co	271.79 d	122.061	85.60
		136.775	10.68
^{58}Co	70.86 d	810.775	99

The experimental cross sections of the Fe(d,x)^{51}Cr, Fe(d,x)^{54}Mn, Fe(d,x)^{56}Mn, Fe(d,x)^{56}Co, Fe(d,x)^{57}Co, and Fe(d,x)^{58}Co reactions are shown in Table III. Since the residual nucleus ^{59}Fe is populated only through the ^{58}Fe(d,p) reaction, the corresponding cross section has been determined using the natural Fe abundance rate. Similar conditions concerned the ^{54}Fe(d,n)^{55}Co, ^{54}Fe(d,α)^{52}Mn, and ^{54}Fe(d,α)^{52}Mn^m reactions at energies up to 20 MeV (Table III), i.e., below the thresholds of reactions on the ^{56}Fe isotope that populate the same residual nuclei. Our measured cross sections, which will be discussed in Sec. IV, are in good agreement with available data within previous works [25–38]. Several comments should concern the following particular reactions.

In contrast to the well explored reaction Fe(d,x)^{56}Co, the excitation function of the Fe(d,x)^{56}Mn reaction is less well known. The reason is that the strong gamma-lines at 846.8 and 1810.77 keV decaying from the nucleus ^{56}Mn interfere with lines from ^{56}Co decay (see Table II). The dependence of the measured activity on the measurement time was fitted by a sum of two exponential functions corresponding to ^{56}Co and ^{56}Mn decays using the MINUIT code [39], and the specific activities of the ^{56}Co and ^{56}Mn nuclei were finally obtained.

While the ^{52}Mn production cross sections are in fact the ^{52}Mn^{m+g} ones, only 1.7% correspond to the isomeric state, being actually within experimental errors. The isomeric state decays mainly through the 1434.07 keV line (see Table II) which interferes with the ^{52}Mn ground state decay. Using a minimization procedure [39], the ^{52}Mn^m cross sections were determined at last.

The ^{58}Co ($T_{1/2}$ = 70.86 d) nucleus has a long-living metastable isomer ^{58}Co^m ($T_{1/2}$ = 9.04 h) decaying through the 24.9 keV (I = 0.0389%) gamma ray, immeasurable by a HPGe detector. Moreover, the ^{58}Co^m isomer feeds the ^{58}Co^g ground state by 100%. Consequently, the activity measurements were performed after the full decay of the metastable state.

Finally, the Fe(d,x)^{51}Cr reaction cross sections are affected by the decay of ^{51}Mn nucleus ($T_{1/2}$ = 46.2 m) which is produced through the Fe(d,x)^{51}Mn reaction. Unfortunately, it has not been possible to determine the latter part within the present experiment. The ^{51}Mn activity cannot be estimated because the corresponding gamma lines are weak (e.g., the intensity of the strongest gamma line of 749.07 keV from the ^{51}Mn decay is 0.26%) while an attempt to separate it from the time dependence of the activity of gammalines following ^{51}Cr decay fails due to relatively large statistical errors.

III. NUCLEAR MODEL ANALYSIS

A. Optical potential assessment

The prime interest for a suitable deuteron OMP is motivated by its further use in the calculations of all deuteron interaction cross sections. Unfortunately, the few measurements of angular distributions of elastic scattered deuterons on

TABLE III. Measured reaction cross sections (mb) for deuterons incident on the ^{nat,54,58}Fe. The energy errors take into account the energy thickness of each foil and the initial-energy spread error. Cross-section errors are composed of statistical errors in activity determination and systematical errors of charge measurement uncertainty (∼5%), foil thickness uncertainty (2%), and uncertainty of HPGe detector efficiency determination (2%). The uncertainties are given in parentheses, in units of the last digit.

Energy	Reaction									
(MeV)	^{54}Fe(d,n)^{55}Co	^{54}Fe(d,α)^{52}Mn	^{54}Fe(d,α)^{52}Mn^{m}	^{58}Fe(d,p)^{59}Fe	Fe(d,x)^{51}Cr	Fe(d,x)^{54}Mn	Fe(d,x)^{56}Mn	Fe(d,x)^{56}Co	Fe(d,x)^{57}Co	Fe(d,x)^{58}Co
4.11 (82)	48.5 (46)	0.57 (15)	1.95 (14)	100 (13)		3.15 (20)	0.37 (4)	0.17 (3)	78.6 (5)	2.45 (15)
5.29 (70)	132 (9)	3.71 (28)	8.76 (57)	273 (23)		13.3 (8)	0.87 (6)	0.22 (3)	232 (14)	6.06 (37)
6.71 (59)	158 (12)	8.10 (59)	17.4 (49)	322 (32)		23.0 (17)	0.99 (15)	0.24 (4)	297 (19)	7.08 (44)
7.62 (55)	153 (11)	15.0 (10)	26.0 (16)	332 (27)		33.9 (20)	1.16 (8)	0.94 (9)	288 (18)	6.77 (41)
8.72 (49)	143 (9)	19.3 (14)	31.8 (20)	320 (35)		43.5 (35)	1.00 (12)	11.3 (10)	271 (22)	6.37 (40)
9.49 (47)	130 (10)	25.1 (17)	35.4 (23)	296 (26)		52.8 (33)	0.92 (7)	52.3 (36)	225 (14)	6.07 (36)
10.45 (44)	112 (9)	27.9 (20)	38.3 (63)	274 (22)	0.18 (5)	61.6 (48)	0.97 (12)	103 (7)	202 (15)	5.67 (41)
11.14 (42)	100 (7)	31.3 (21)	35.7 (23)	254 (22)	0.54 (7)	67.1 (40)	0.98 (8)	161 (10)	164 (10)	5.55 (33)
11.99 (39)	92.2 (57)	32.4 (25)	36.0 (77)	239 (31)	0.97 (52)	69.4 (42)	1.15 (21)	198 (13)	155 (10)	5.47 (32)
12.62 (38)	83.0 (57)	31.1 (21)	27.9 (28)	226 (21)	1.70 (13)	65.4 (39)	1.27 (10)	234 (14)	130 (8)	5.22 (31)
13.40 (36)	76.7 (47)	31.2 (28)	30.3 (86)	199 (20)	2.34 (19)	61.8 (48)	2.17 (28)	251 (17)	127 (8)	5.16 (35)
13.99 (36)	71.5 (47)	27.7 (21)	27.1 (20)	184 (30)	2.94 (32)	56.6 (35)	3.29 (23)	267 (17)	106 (7)	4.78 (29)
14.71 (34)	66.7 (41)	25.7 (27)	28.7 (24)	171 (58)	3.77 (31)	54.1 (37)	4.18 (61)	286 (21)	105 (9)	4.87 (31)
14.72 (34)	62.8 (37)	22.9 (14)		170 (13)	3.88 (26)	52.4 (31)	3.96 (51)	292 (17)	100 (6)	4.64 (28)
15.27 (33)	66.5 (41)	22.4 (16)		162 (20)	4.41 (33)	51.0 (31)	5.69 (43)	285 (17)	92.9 (55)	4.62 (28)
15.95 (33)	60.3 (41)	22.1 (16)		158 (38)	4.90 (36)	48.8 (30)	6.85 (51)	308 (22)	91.1 (58)	4.62 (30)
16.47 (31)	59.7 (42)			145 (17)	5.93 (40)	46.4 (28)	8.15 (63)	289 (18)	82.7 (50)	4.44 (27)
17.11 (31)	55.9 (33)			143 (14)	6.55 (45)	43.1 (25)	9.09 (54)	318 (19)	89.4 (52)	4.22 (25)
17.13 (31)	51.7 (30)			146 (13)	6.12 (38)	42.2 (25)	9.74 (79)	321 (18)	78.9 (46)	4.05 (24)
18.23 (29)				131 (22)	7.12 (51)	41.1 (25)	11.8 (13)	320 (21)	74.9 (53)	3.89 (26)
18.69 (29)				122 (20)	7.48 (48)	39.2 (24)	15.8 (11)	313 (19)	68.4 (41)	3.69 (22)
19.29 (28)				121 (19)	7.56 (50)	37.7 (27)	15.5 (12)	302 (20)	65.6 (49)	3.36 (23)
19.35 (28)				110 (11)	7.74 (47)	37.1 (22)	15.6 (11)	305 (17)	65.4 (38)	3.35 (20)
19.74 (28)				123 (16)	8.82 (58)	37.9 (23)	20.6 (15)	277 (17)	62.6 (41)	3.37 (21)

^{54,56,58}Fe [40], but none on ^{57}Fe, do not allow an extended OMP analysis.

The choice of the optical potential for the deuteron-induced activation of ^{nat}Fe calculations has been based on the simultaneous analysis of the deuteron elastic scattering and deuteron total-reaction cross section. Consequently, these experimental data have been compared with the corresponding predictions given by various global OMPs [41–45]. Thus, the predictions of Perey and Perey [41], Lohr-Haeberly [42], Daehnick *et al.* [43], Bojowald *et al.* [44], and Haixia-Cai [45] global optical potentials for elastic-scattering angular distributions of deuterons on ^{54,56,58}Fe are shown in Figs. 1 and 2. The best description of the elastic scattering angular distributions, along the large incident energy interval 5–60 MeV, is given by the Daehnick *et al.* [43] optical potential. Concerning the description by the same global optical potentials [41–45] of the deuteron total-reaction cross sections, measured at only one energy for each of the ^{54,56,58}Fe isotopes, the results shown in Fig. 2 cannot change the assessment of the Daehnick *et al.* [43] potential for ^{nat}Fe deuteron-activation cross-section calculation.

B. Deuteron breakup effects on activation cross sections

The physical picture of the deuteron breakup in the Coulomb and nuclear fields of the target nucleus considers two distinct processes, namely the elastic breakup (EB) in which the target nucleus remains in its ground state and none of the deuteron constituents interacts with it, and the inelastic breakup or breakup fusion (BF), where one of these deuteron constituents interacts with the target nucleus while the remaining one is detected.

The former parametrization of the total nucleon-emission breakup cross sections was given by Kalbach [46] as a function of the deuteron incident energy E and mass number A of the target nucleus:

$$\sigma_{BU}^{b} = K_{d,b}\frac{(A^{1/3}+0.8)^2}{1+\exp\left(\frac{13-E}{6}\right)}, \quad K_{d,p}=21, \quad K_{d,n}=18. \tag{1}$$

The corresponding total proton-emission breakup cross sections for deuteron interactions with ^{54,56,57}Fe are shown in Fig. 3.

Additional features of the breakup cross-section parametrization in terms of the deuteron total-reaction cross section σ_R have been considered by Avrigeanu *et al.* [1], namely the dependence on the target charge number Z, while distinct forms are provided for the total BU nucleon emission

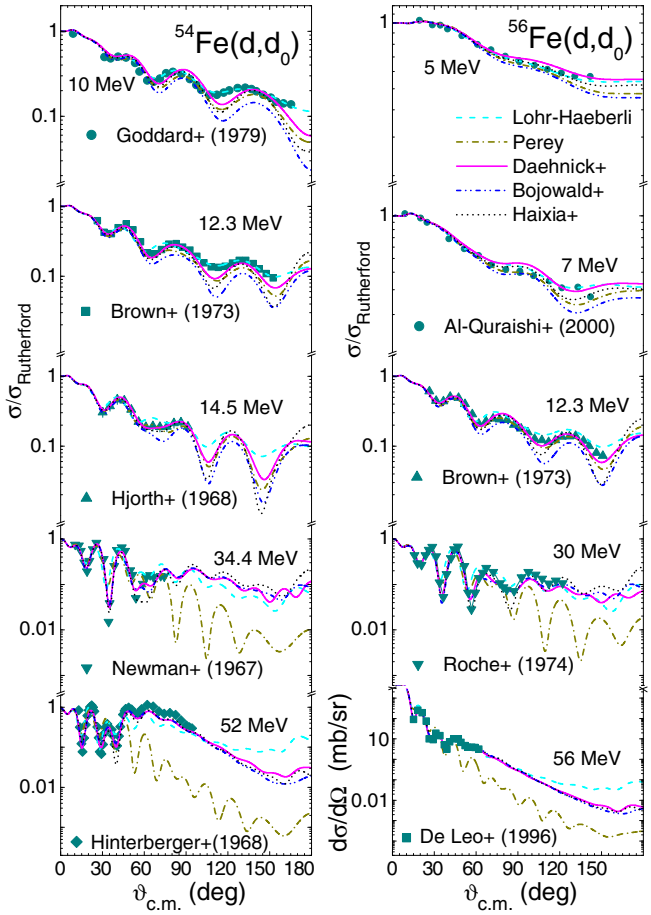

FIG. 1. (Color online) Comparison of measured [40] and calculated elastic-scattering angular distributions of deuterons on ^{54}Fe (left side) and ^{56}Fe (right side), from 5 to ∼60 MeV, using the global OMPs of Refs. [41–45].

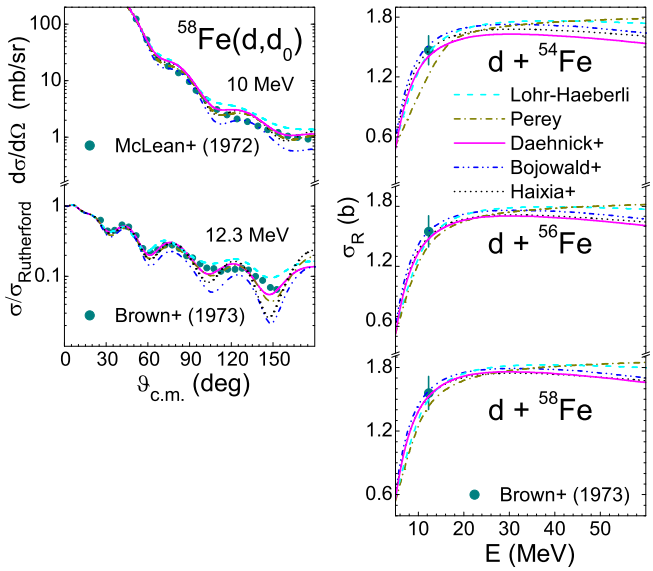

FIG. 2. (Color online) (Left) As for Fig. 1 but for the target nucleus ^{58}Fe [40]. (Right) Comparison of measured [40] and calculated total reaction cross sections of deuterons incident on ^{54,56,58}Fe from 5 to ∼60 MeV, using the global OMPs of Refs. [41–45].

as well as the EB and BF components (Fig. 3):

$$\sigma_{BU}^{p/n} = [0.087 - 0.0066Z + 0.00163ZA^{1/3} + 0.0017A^{1/3}E - 0.000002ZE^2]\sigma_R, \quad (2)$$

$$\sigma_{EB} = [0.031 - 0.0028Z + 0.00051ZA^{1/3} + 0.0005A^{1/3}E - 0.000001ZE^2]\sigma_R, \quad (3)$$

$$\sigma_{BF}^{p/n} = \sigma_{BU}^{p/n} - \sigma_{EB}, \quad (4)$$

leading to the total-breakup cross section

$$\sigma_{BU} = \sigma_{EB} + 2\sigma_{BF}^{p/n}. \quad (5)$$

Equal BF cross sections for proton and neutron emission have been considered in the above expressions.

The latest BU parametrization, given by Kalbach [47] within the FENDL-3 project [10], considers also equal cross sections for the BU proton and neutron emission:

$$\sigma_{BU}^{p/n}(E) = 5.4(D_0)^2 \exp\left(\frac{E}{170}\right)\left[1 + \exp\left(\frac{42 - E}{14}\right)\right]^{-1}, \quad (6)$$

where

$$D_0 = 1.2\frac{5A^{\frac{1}{3}}}{1 + \exp\left(\frac{E}{30}\right)} + 1.2.$$

As can be seen in the upper part of Fig. 3, both of Kalbach's parametrizations [46,47] predict similar higher values of total proton breakup cross sections at the lowest incident energies, even exceeding σ_R, while the latter predicts also lower values in comparison with the experimental systematics of the total proton-emission breakup fraction σ_{BU}^p/σ_R [48–51] for E from ∼10 to 60 MeV (Fig. 4). Regardless the differences between the Kalbach [46] and Avrigeanu *et al.* [1] predictions at low deuteron energies, they result in a similar trend of the two approaches for the total proton-emission breakup excitation

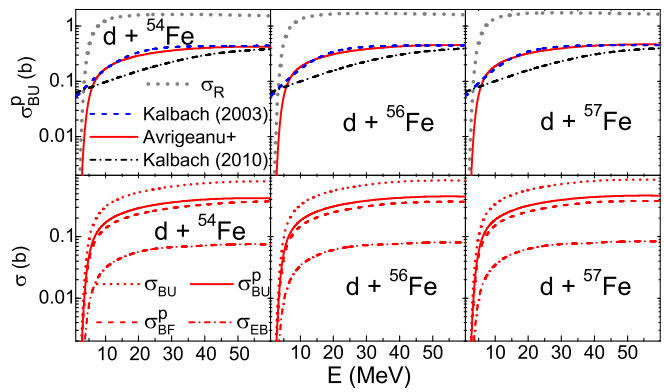

FIG. 3. (Color online) The energy dependence of the deuteron total reaction cross sections [43] (dotted curves) and the total proton-emission breakup cross sections given by parametrizations of Refs. [1] (solid curves), [46] (dashed curves), and [47] (dash-dotted curves), for deuteron interactions with ^{54,56,57}Fe (upper row). The energy dependence of the total BU (dotted curves), BU nucleon emission (solid curves), BF (dashed curves), and EB (dash-dotted curves) cross sections [1] for the deuteron interactions with the same Fe isotopes (lower row).

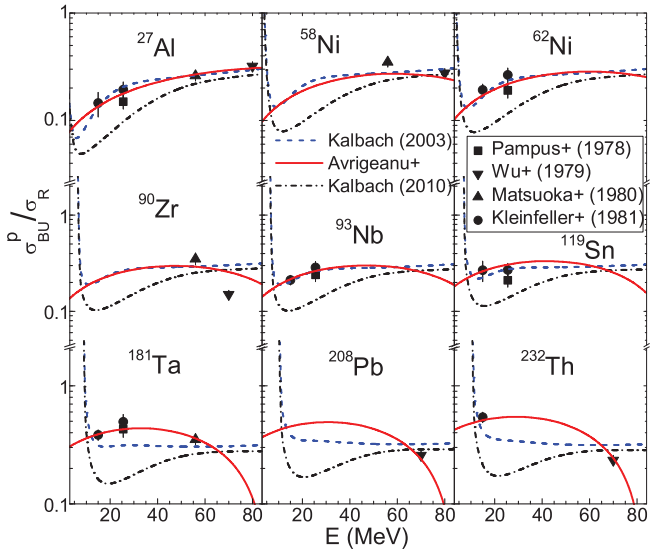

FIG. 4. (Color online) Comparison of experimental [48–51] total proton-emission breakup fraction and the corresponding parametrizations of Refs. [1] (solid curves), [46] (dashed curves), and [47] (dash-dotted curves), for deuteron interactions with ^{27}Al, ^{58,62}Ni, ^{90}Zr,^{93}Nb, ^{119}Sn, ^{181}Ta, ^{208}Pb, and ^{232}Th.

functions within the energy range ∼10–60 MeV. The very scarce experimental deuteron BU systematics [48–52] may lead to large uncertainties of the BU cross-section energy dependence at deuteron energies over 60 MeV. Thus, only the extension of experimental data beyond this energy limit may improve the corresponding parametrizations. They would be of interest for basic research while the needs of the actual strategic research programs [7–9] did not go over this limit.

Overall, there are actually two opposite effects of the deuteron breakup on the deuteron activation cross sections that should be considered. Firstly, the total-reaction cross section, that is shared among different outgoing channels, is reduced by the value of the total breakup cross section σ_{BU}. On the other hand, the BF component, where one of the deuteron constituents interacts with the target nucleus, leading to a secondary composite nucleus, brings contributions to different reaction channels [1,2,4–6,11,12,14,16,21,22]. Thus, the absorbed proton or neutron following the deuteron breakup contributes to the enhancement of the corresponding (d,xn) or (d,xp) reaction cross sections, respectively.

In order to calculate the BF enhancement of, e.g., the (d,xn) reaction cross sections, the BF proton-emission cross section σ^p_{BF} should be multiplied by the ratios $\sigma_{(p,x)}/\sigma^p_R$, corresponding to the above-mentioned enhancing reaction, convoluted with the Gaussian line shape distribution of the BF proton energy E_p for a given deuteron incident energy E. Finally, the integration over the BF proton energy provides the BF enhancement cross section [4–6,21,22]:

$$\sigma^{p,x}_{BF}(E) = \sigma^p_{BF}(E) \int dE_p \frac{\sigma_{(p,x)}(E_p)}{\sigma^p_R} \times \frac{1}{(2\pi)^{\frac{1}{2}} w} \exp\left[- \frac{\left[E_p - E^0_p(E)\right]^2}{2w^2} \right], \quad (7)$$

where σ^p_R is the proton total reaction cross section, x stands for various outgoing channels, e.g., γ, n, d, or α, while E^0_p and w are the centroid and standard deviation, respectively, of the above-mentioned BU proton-energy Gaussian distribution given by Kalbach [46] related parameters. Interpolated values of the experimental nucleon-induced reaction cross sections from EXFOR library [53] have been involved within the BU enhancement estimation, e.g., Refs. [5,14], in order to reduce as much as possible the supplementary uncertainties brought by additional theoretical calculations.

The BF enhancements brought by BU protons and neutrons emitted during the deuteron interaction with ^{nat}Fe, through the (p,γ), (p,n), $(p,2n)$, $(p,3n)$, $(p,2p)$, (p,α), $(p,\alpha n)$, (n,γ), (n,d), and (n,α) reactions populating various residual nuclei, are shown in Figs. 8–18.

C. Transfer reactions

Apart from the breakup contributions to deuteron interactions, increased attention has to be paid to the direct reactions, so far very poorly considered within deuteron activation analysis. Since the interactions of deuterons on low and medium mass target nuclei at energies around the Coulomb barrier proceed largely through the DR mechanism, their contribution is important for the first-chance emitted particle cross section. On the other hand, similarly to the breakup mechanism, the transfer reactions that enhance some residual excitation functions decrease the deuteron flux going towards statistical processes. The assessment of the total transfer reaction cross section is mandatory in this case, but it is conditioned by the available experimental spectroscopic factors or at least outgoing particle angular distributions.

The appropriate calculations of the DR stripping and pick-up mechanism contributions, that are important at the low energy side of the (d,p), (d,n), (d,t), and (d,α) excitation functions [1,2,4,6,11,14,16,21,22,54], have been performed in the frame of the CRC formalism by using the code FRESCO [17]. The post/prior form distorted-wave transition amplitudes, for $(d,n/p)$ and respectively $(d,t/\alpha)$ reactions, and the finite-range interaction have been considered. The n-p effective interaction in the deuteron [55] as well as the d-n effective interaction in the triton [56] are assumed to have a Gaussian shape, while the Woods-Saxon shape [57] has been considered for the d-d effective interaction in the alpha particle. The transferred nucleon and deuteron bound states were generated in a Woods-Saxon real potential [1,4,6,21]. Concerning the (d,α) pick-up cross section calculation, the transfer of the deuteron cluster has been taken into account. The populated discrete levels and the corresponding spectroscopic factors for each DR type considered, e.g., [58–60] for (d,n) and (d,p) stripping processes, and [58,61–64] for (d,t) and (d,α) pick-up processes, have been obtained from the ENSDF library; see [65] and references therein.

Actually, the one-nucleon transfer reactions, e.g., (d,n) and (d,p) stripping processes, have been of critical importance for the nuclear structure studies. Thus, the spectroscopic factors extracted from the analysis of experimental angular distributions of the corresponding emitted particles did contribute to the validation of the nuclear shell model. Consequently,

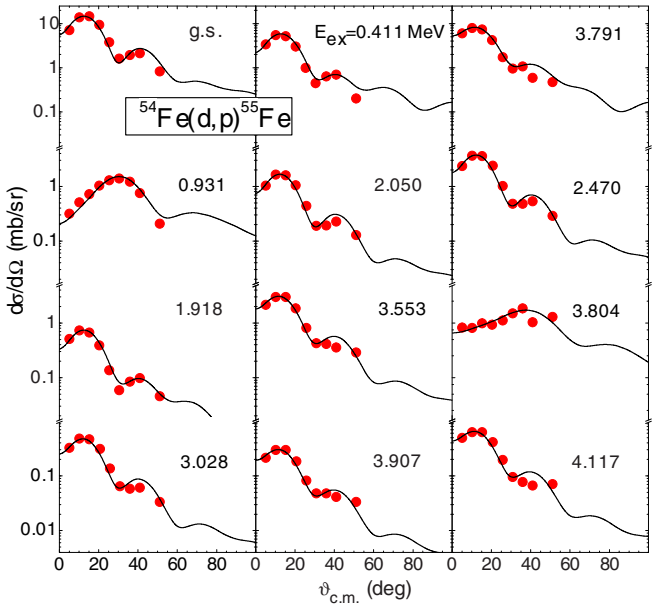

FIG. 5. (Color online) Comparison of measured [66] and calculated (solid curves) proton angular distributions from the ^{54}Fe$(d,p)^{55}$Fe stripping reaction at $E = 14$ MeV.

the systematics of the achieved experimental spectroscopic factors makes possible the calculation of almost total (d,n) and (d,p) cross-section contributions to the deuteron activation. Unfortunately this is not the case of the pick-up (d,t) and (d,α) studies, for which the experimental *triton* and α-particle angular distributions as well as spectroscopic factors are extremely scarce, so that the corresponding cross sections for each of the Fe isotopes cannot be estimated or at best could be underestimated.

An entire analysis of the DR contributions is shown in Figs. 5 and 6 for deuteron interactions with ^{54}Fe. Thus, we have considered the population of 44 levels of the ^{55}Fe nucleus [58,66] within a similar analysis of the ^{54}Fe$(d,p)^{55}$Fe stripping cross section. The appropriate description of the corresponding proton angular distributions, e.g., Fig. 5, validates the correctness of the theoretical stripping excitation function shown in Fig. 6(a). Moreover, the suitable description of angular-distribution maximum values of neutron [67] and α particles [68] has also supported the calculations of the

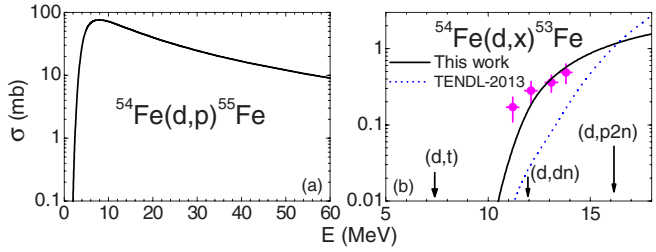

FIG. 6. (Color online) (a) Calculated cross sections of the ^{54}Fe$(d,p)^{55}$Fe stripping reaction, and (b) comparison of the measured [69], presently calculated (solid curves), and TENDL-2013 [19] (dotted curves) cross sections of the ^{54}Fe$(d,x)^{53}$Fe reaction. The (d,t), (d,dn), and $(d,p2n)$ reaction thresholds are also shown (arrows).

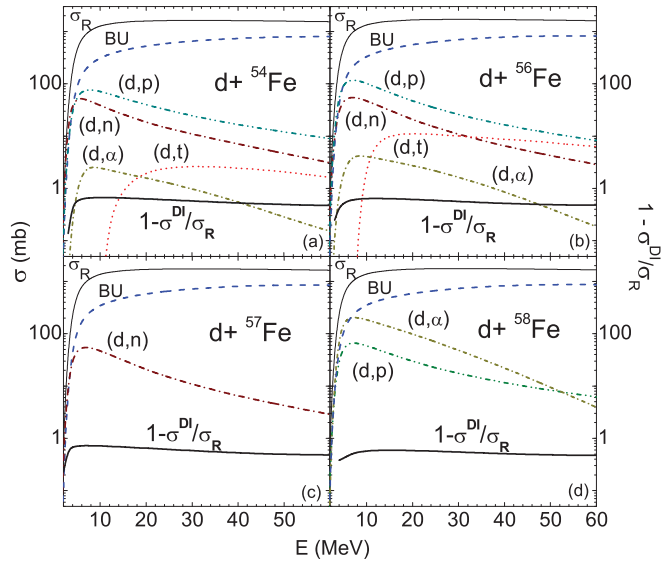

FIG. 7. (Color online) Total-reaction (thin solid curves), BU (dashed curves), stripping (d,n) (dash-dotted curves) and (d,p) (dash-dot-dotted curves), and pick-up (d,t) (dotted curves) and (d,α) (short dash-dotted curves) reaction cross sections for deuterons on ^{54,56,57,58}Fe, and the corresponding reduction factors of the deuteron flux going towards statistical processes (thick solid curves).

total DR cross section that are shown in Fig. 7(a) for the ^{54}Fe isotope.

A particular note should concern the (d,t) pick-up contribution to the total (d,t) activation cross section. In spite of being usually neglected in deuteron activation cross-sections calculations, the (d,t) pick-up process is responsible for the lowest-energy side of the excitation function, namely at the energies between its threshold and those of the (d,dn) and $(d,p2n)$ reactions that contribute to the population of the same residual nucleus. These threshold energies are shown in Fig. 6(b) for a better understanding of the pick-up reactions' important role within deuteron interactions at low incident energies. At the same time, the suitable description of the measured (d,t) excitation function [69] validates the present pick-up (d,t) cross-sections calculation.

Finally, we have taken into account the deuteron total reaction cross section that remains available for the PE + CN mechanisms, following the correction for the incident flux leakage through direct interactions (DI), i.e., the breakup, stripping, and pick-up, as given by a reduction factor:

$$1 - \frac{\sigma_{BU} + \sigma_{(d,n)} + \sigma_{(d,p)} + \sigma_{(d,t)} + \sigma_{(d,\alpha)}}{\sigma_R} = 1 - \frac{\sigma^{DI}}{\sigma_R}. \quad (8)$$

The energy dependence of this reduction factor, as well as of its components corresponding to deuteron interactions with the ^{54,56,57,58}Fe isotopes, is shown in Fig. 7.

The significant effect of the stripping (d,p), (d,n), and pick-up (d,α), (d,t) reactions for the deuteron interaction with Fe isotopes is proved in Figs. 8(b), 9(b), 11(b), 12(b), 14(b), 15(b), 16(c), 17(a), and 17(c).

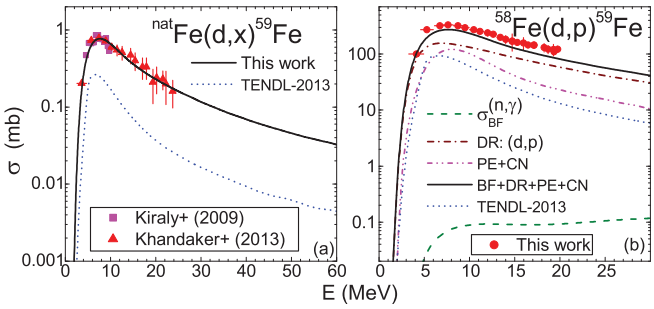

FIG. 8. (Color online) Comparison of previous [25,26] and present (solid circles) measurements, TENDL-2013 [19] predictions (dotted curves), and present calculation (solid curves) of cross sections for (a) ^{nat}Fe$(d,x)^{59}$Fe and (b) ^{58}Fe$(d,p)^{59}$Fe reactions, along with inelastic breakup enhancement (dashed curves), stripping (d,p) reaction (dash-dotted curve), and PE + CN components (dash-dot-dotted curves) corrected for initial deuteron flux leakage through DI (see text).

D. Statistical emission

The PE and CN processes become important with the increase of the incident energy above the Coulomb barrier. We have calculated the corresponding reaction cross sections by means of the TALYS-1.4 code [18], taking into account also the above-discussed breakup, stripping, and pick-up results through the reduction factor of Eq. (8).

The following options of the TALYS-1.4 input have been used: (a) the optical model potentials of Koning-Delaroche [70], Daehnick *et al.* [43], Avrigeanu *et al.* [71], and Becchetti-Greenlees [72] for neutrons, protons, deuterons, alpha-particles and tritons, respectively; (b) the back-shifted Fermi gas (BSFG) formula for the nuclear level density; (c) no TALYS breakup contribution, since the above-mentioned breakup components were considered for both the total-reaction cross-section reduction factor and the BF enhancements account; (d) the preequilibrium transition rates calculated by means of the corresponding OMP parameters, using the value 3 for the *preeqmode* TALYS keyword.

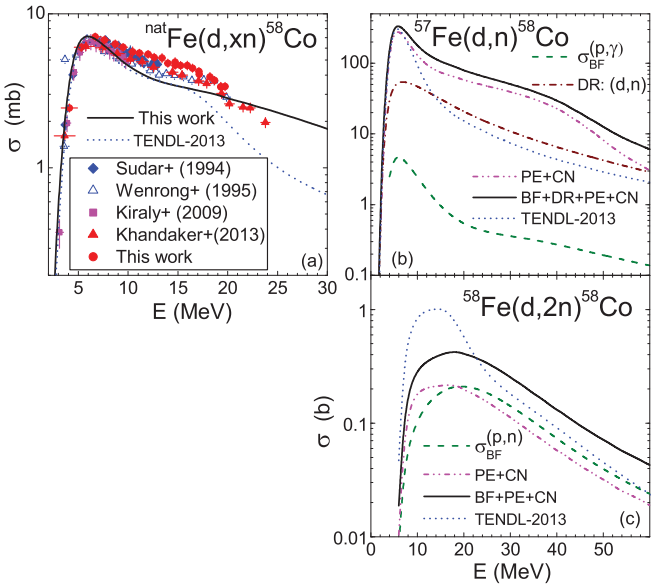

FIG. 9. (Color online) Comparison of previous [25–28] and present (solid circles) measurements, TENDL-2013 [19] predictions (dotted curves), and present calculations (solid curves) of cross sections for (a) the ^{nat}Fe$(d,xn)^{58}$Co, (b) ^{57}Fe$(d,n)^{58}$Co, and (c) ^{58}Fe$(d,2n)^{58}$Co reactions, along with inelastic breakup enhancement (dashed curves), stripping (d,n) reaction (dash-dotted curve), and PE + CN components (dash-dot-dotted curves) corrected for initial deuteron flux leakage through DI (see text).

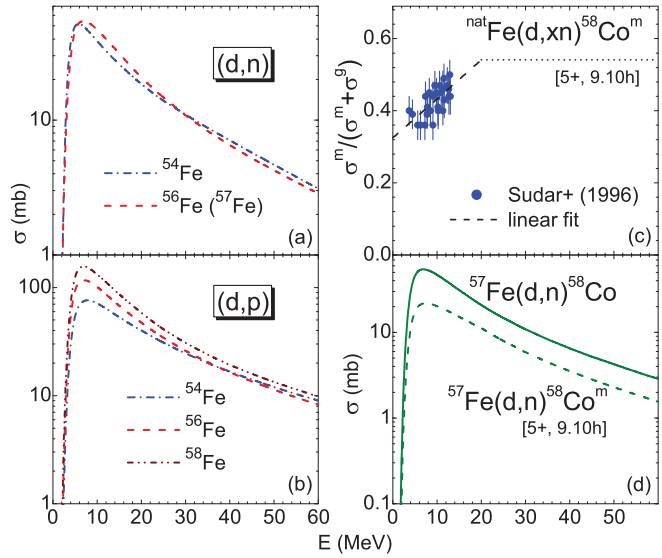

FIG. 10. (Color online) (a),(b) Calculated cross sections of Fe isotopes for stripping reactions (d,n) and (d,p), respectively, (c) experimental isomeric cross-section ratios of the ^{nat}Fe$(d,xn)^{58}$Co^{m,g} reaction [29] as well as the linear interpolation (dashed curve) and constant extrapolation for $E > 20$ MeV (dotted line), and (d) the derived stripping component of the ^{nat}Fe$(d,xn)^{58}$Co^{m} reaction cross sections (dashed curve).

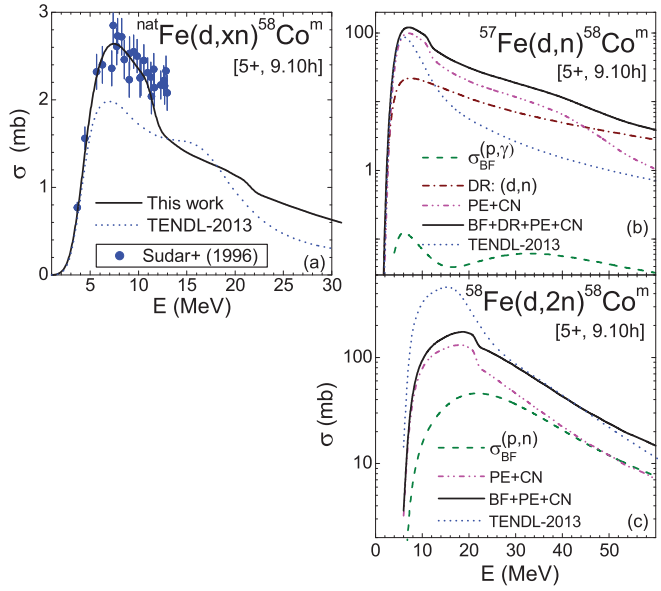

FIG. 11. (Color online) Same as Fig. 9 but for (a) ^{nat}Fe$(d,xn)^{58}$Co^{m} [28], (b) ^{57}Fe$(d,n)^{58}$Co^{m}, and (c) ^{58}Fe$(d,2n)^{58}$Co^{m} reactions.

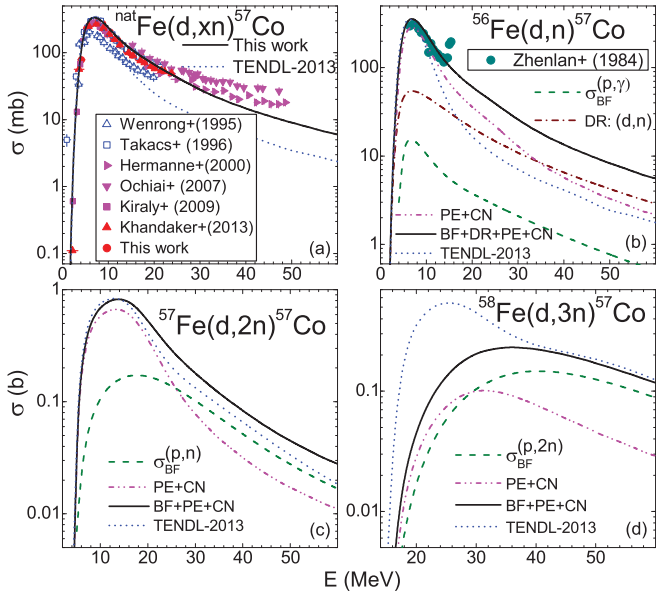

FIG. 12. (Color online) Same as Fig. 9 but for (a) ^{nat}Fe$(d,xn)^{57}$Co [25–27,30–32], (b) ^{56}Fe$(d,n)^{57}$Co [33], (c) ^{57}Fe$(d,2n)^{57}$Co, and (d) ^{58}Fe$(d,3n)^{57}$Co reactions.

IV. RESULTS AND DISCUSSION

The detailed contributions of various isotopes to a certain activation excitation function of the deuteron interactions with ^{nat}Fe are compared in Figs. 8–18 with the measured cross sections given in Sec. II and formerly available [25–38] as

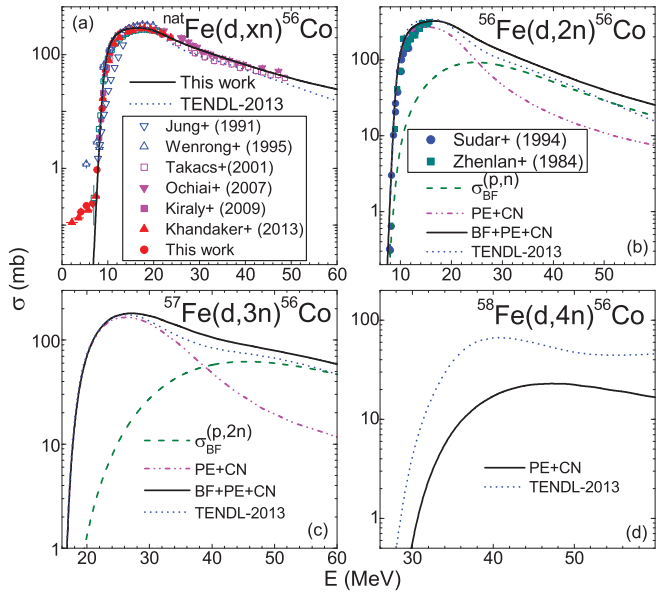

FIG. 13. (Color online) Comparison of previous [25–28,32–35] and present (solid circles) measurements, TENDL-2013 [19] predictions (dotted curves), and present calculations (solid curves) of cross sections for (a) ^{nat}Fe$(d,xn)^{56}$Co, (b) ^{56}Fe$(d,2n)^{56}$Co, (c) ^{57}Fe$(d,3n)^{56}$Co, and (d) ^{58}Fe$(d,4n)^{56}$Co reactions, along with inelastic breakup enhancement (dashed curves), and PE + CN components (dash-dot-dotted curves) corrected for initial deuteron flux leakage through DI (see text).

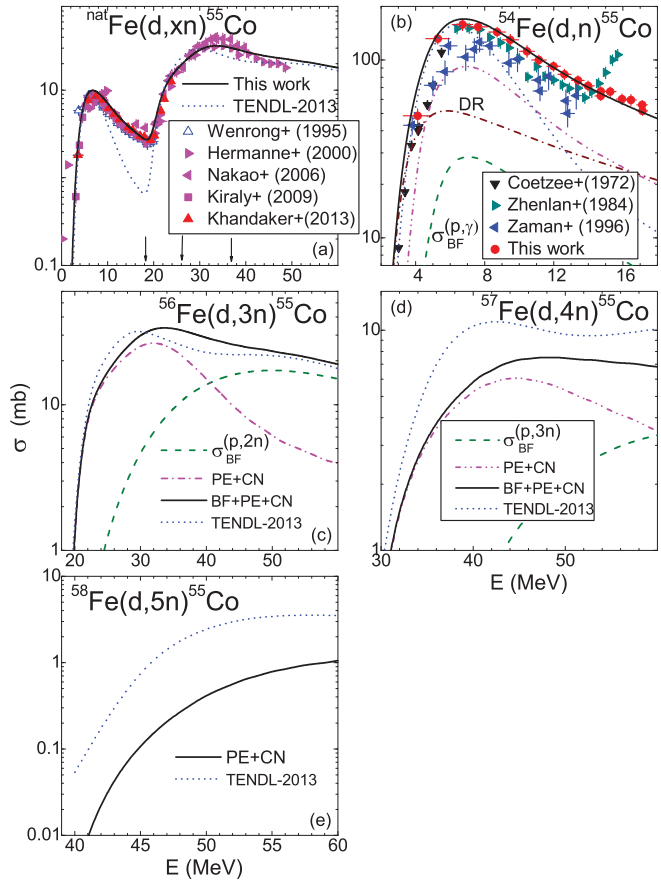

FIG. 14. (Color online) Same as Fig. 9 but for (a) the ^{nat}Fe$(d,xn)^{55}$Co reaction [25–27,31,36], with the arrows corresponding to the (d,xn) reaction thresholds, where $x = 3, 4$, and 5, and for (b) ^{54}Fe$(d,n)^{55}$Co [33,37,38], (c) ^{56}Fe$(d,3n)^{55}$Co, (d) ^{57}Fe$(d,4n)^{55}$Co, and (e) ^{58}Fe$(d,5n)^{55}$Co reactions.

well as with the TENDL-2013 predictions [19], while a global comparison of the data and calculated results for ^{nat}Fe is shown in Fig. 19. The overall agreement of experimental and calculated activation excitation functions supports the correctness of the reaction mechanism descriptions that have been considered for the deuteron-nucleus interactions, while particular comments concern several categories.

A. The (d,n) and (d,p) reactions

The description of measured excitation functions corresponding to deuteron interaction with a mono-isotopic Fe target and one-nucleon emission, namely ^{54,56}Fe(d,n)^{55,57}Co and ^{58}Fe(d,p)^{59}Fe reactions, represents in particular a distinct test of the nuclear model approach. Of major importance in this respect is the (d,p) reaction on ^{58}Fe nucleus [Fig. 8(b)], due to the large contribution of the stripping reaction mechanism whose consideration is critical for the suitable account of the measured cross sections. A different case is that of the (d,n) reaction on ^{54,56}Fe target nuclei, Figs. 12(b) and 14(b), respectively, due to the quite larger neutron statistical (PE + CN) emission that goes mainly to population of this reaction

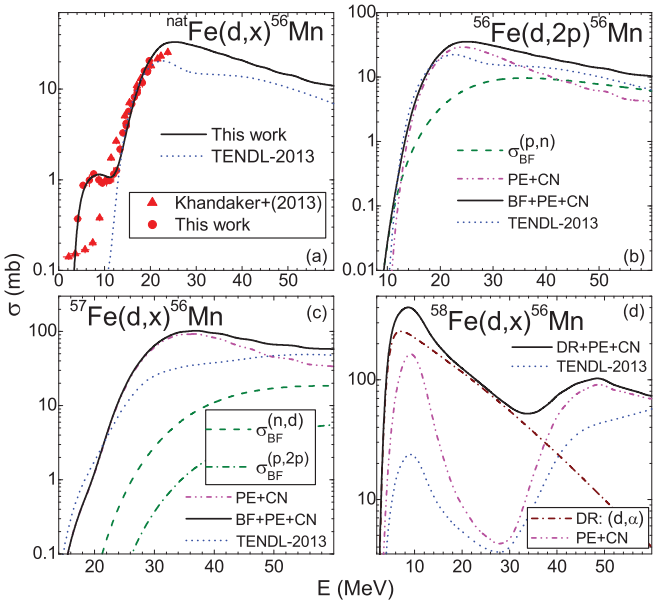

FIG. 15. (Color online) Comparison of previous [26] and present (solid circles) measurements, TENDL-2013 [19] predictions (dotted curves), and present calculations (solid curves) of cross sections for (a) ^{nat}Fe$(d,x)^{56}$Mn, (b) ^{56}Fe$(d,2p)^{56}$Mn, (c) ^{57}Fe$(d,x)^{56}$Mn, and (d) ^{58}Fe$(d,x)^{56}$Mn reactions, along with inelastic breakup enhancement (dashed curves), pick-up (d,α) reaction (dash-dotted curve), and PE + CN components (dash-dot-dotted curves), corrected for initial deuteron flux leakage through DI (see text).

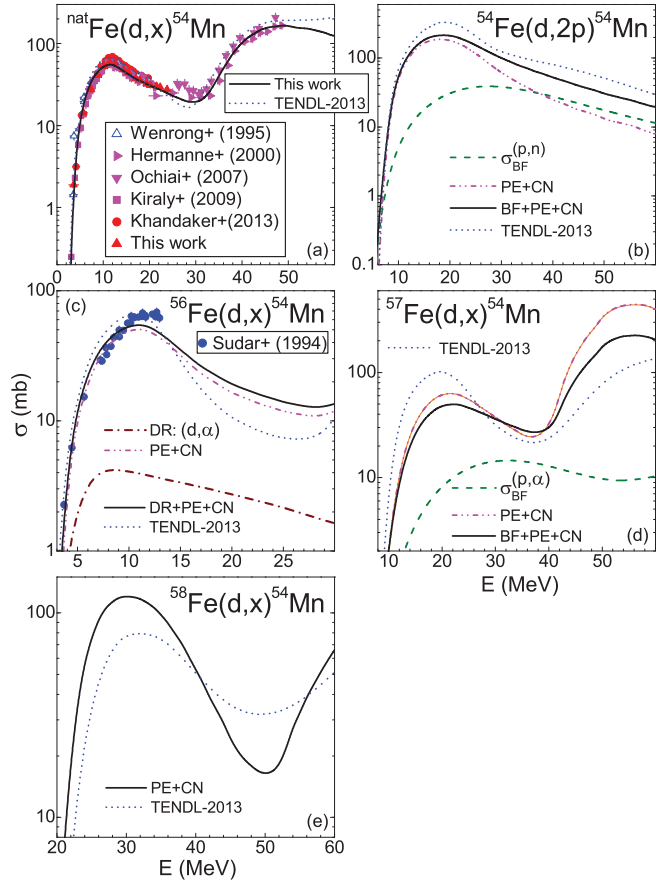

FIG. 16. (Color online) Same as Fig. 15 but for (a) ^{nat}Fe$(d,x)^{54}$Mn [25–27,31,32], (b) ^{54}Fe$(d,2p)^{54}$Mn, (c) ^{56}Fe$(d,x)^{54}$Mn [28], (d) ^{57}Fe$(d,x)^{54}$Mn, and (e) ^{58}Fe$(d,x)^{54}$Mn reactions.

channel until the $(d,2n)$ reactions becomes dominant at higher energies. Then again the stripping reaction plays the key role.

An analysis requesting additional assumptions concerns the total and isomeric state activations of the ^{58}Co residual nucleus shown in Figs. 9(b) and 11(b), respectively. Since any specific experimental information needed for the estimation of the stripping (d,n) contribution to the ^{57}Fe$(d,n)^{58}$Co interaction process—e.g., neutron angular distributions or spectroscopic factors corresponding to populations of various excited levels of ^{58}Co through the stripping mechanism—is not available, an estimation of this contribution has been necessary. Thus, we have considered the same stripping contribution for ^{56,57}Fe, as shown in Fig. 10(a). Actually, one may see in Fig. 10(a) that the (d,n) stripping cross sections increase with the isotopic mass while their excitation-function maximum moves toward higher energies. Therefore, taking into account equal (d,n) stripping contributions for ^{56,57}Fe isotopes, we may have at least the lowest limit estimation of the ^{57}Fe(d,n) stripping excitation function shown in both Figs. 9(b) and 10(d). Moreover, we deduced the stripping contribution to the ^{58}Co^m activation shown in Fig. 10(d) by using the experimental ratio $\sigma^m/(\sigma^m+\sigma^g)$ of the isomeric state population to the sum of isomeric and ground states population through the ^{nat}Fe$(d,xn)^{58}$Co reaction [29], as well as a linear interpolation of the measured ratios and the assumption of a constant ratio value of 0.541 above the incident energy of 20 MeV [Fig. 10(c)]. Finally, the results of these approximations describe satisfactorily the ^{58}Co^m activation excitation function shown in Fig. 11(a). However, increased values would be necessary in the case of ^{58}Co activation for the agreement with the experimental excitation function shown in Fig. 9(a). Nevertheless, such an eventual increase could be well motivated since we considered only the lowest limit of the stripping contribution for the ^{57}Fe target nucleus.

One may note that the nuclear model analysis of the ^{54}Fe$(d,n)^{55}$Co reaction [Fig. 14(b)] has pointed out that the apparent discrepancies between TENDL-2013 [19] and the experimental data could be due to the DI weak treatment. The complete analysis of this activation excitation function illustrates indeed the complexity of the deuteron interactions involving breakup, stripping, and PE and CN reaction mechanisms. As a result of the energy thresholds for the rest of the Fe isotopes [shown in Fig. 14(a) for the $(d,3n)$, $(d,4n)$, and $(d,5n)$ reactions], this reaction is the only one contributing to the ^{nat}Fe$(d,xn)^{55}$Co excitation function for incident energies $\leqslant$18.3 MeV. Consequently, the effects of breakup and stripping mechanisms are better emphasized in the absence of strong contributions coming from the 91.8% most abundant ^{56}Fe isotope.

B. The $(d,2n)$ and $(d,3n)$ reactions

These reactions become consecutively the dominant channels above the deuteron energies of ∼20 MeV. The statistical

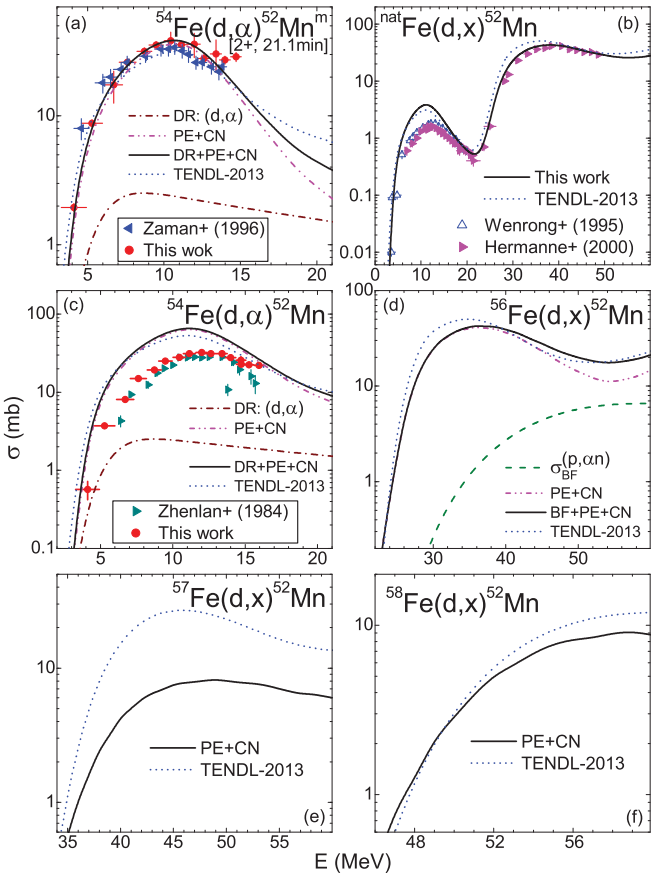

FIG. 17. (Color online) Same as Fig. 15 but for (a) ^{54}Fe$(d,\alpha)^{52}$Mn^{m} [37], (b) ^{nat}Fe$(d,x)^{52}$Mn [27,31], (c) ^{54}Fe$(d,\alpha)^{52}$Mn [33], (d) ^{56}Fe$(d,x)^{52}$Mn, (e) ^{57}Fe$(d,x)^{52}$Mn, and (f) ^{58}Fe$(d,x)^{52}$Mn reactions.

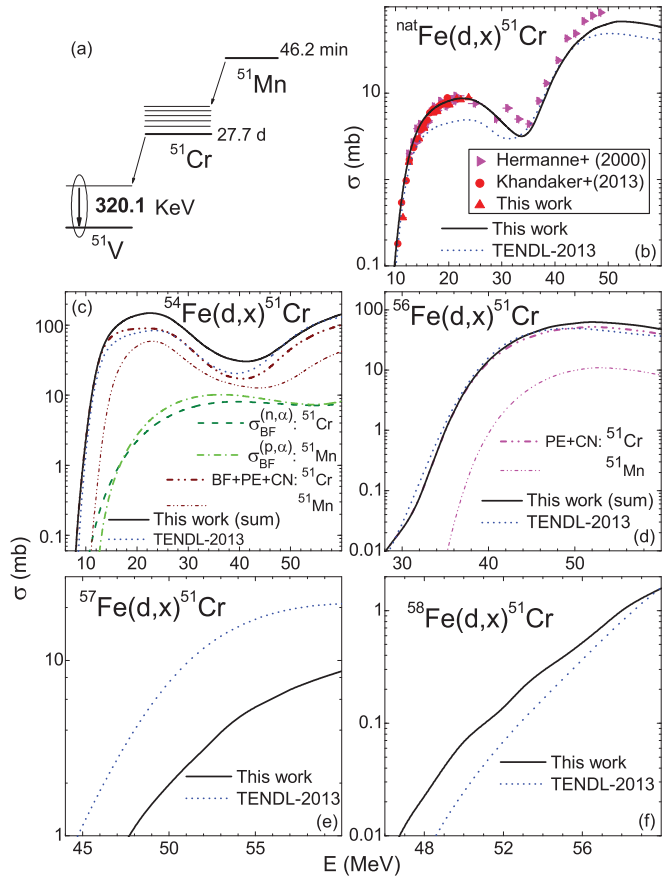

FIG. 18. (Color online) (a) Schematic decay of ^{51}Mn and ^{51}Cr nuclei [65,73–75]; comparison of previous [26,31] and present (solid circles) measurements, present calculations (solid curves), and TENDL-2013 [19] predictions (dotted curves) of cross sections, for (b) ^{nat}Fe$(d,x)^{51}$Cr, (c) ^{54}Fe$(d,x)^{51}$Cr, (d) ^{56}Fe$(d,x)^{51}$Cr, (e) ^{57}Fe$(d,x)^{51}$Cr, and (e) ^{58}Fe$(d,x)^{51}$Cr reactions, along with BF enhancement reactions ^{54}Fe$(n,\alpha)^{51}$Cr (dashed curve) and ^{54}Fe$(p,\alpha)^{51}$Mn (dash-dotted curve) and PE and CN components for ^{51}Cr (thick dash-dot-dotted curves) and ^{51}Mn (thin dash-dot-dotted curves) residual nuclei (see text).

(PE + CN) emission gives the largest contribution to these yields only at the beginning of the corresponding excitation functions, during their increase with the incident energy. Next, the decrease of these functions becomes slower due to larger contributions brought by the inelastic breakup through the (p,n) and $(p,2n)$ processes (Figs. 9, 11, 12, 13, and 14). The correctness of this sum is proved by the experimental cross sections for the $(d,2n)$ reaction on the ^{56}Fe nucleus [Fig. 13(b)], which is the only one of this kind measured on a mono-isotopic Fe target.

C. The $(d,\alpha x)$ reactions

The comparison of the calculated and measured cross sections for ^{56}Fe(d,α)^{54}Mn [Fig. 16(c)], ^{54}Fe(d,α)^{52}Mn^{m} and ^{54}Fe(d,α)^{52}Mn [Figs. 17(a) and 17(c)] reactions on monoisotopic Fe targets shows that the (d,α) pick-up component is less important than the stripping one for the (d,p) reaction. The agreement found for the first two of the above-mentioned reactions, strengthened by that for the ^{54}Mn and ^{52}Mn activation induced on ^{nat}Fe (Figs. 16 and 17), support consistently the present model calculations. At the same time, the dominant pick-up component for the ^{58}Fe(d,α)^{56}Mn reaction [Fig. 15(d)] is supported by the agreement shown in Fig. 15(a) for the ^{56}Mn activation induced on ^{nat}Fe at the energies below the thresholds for the $(d,2p)$ and $(d,n2p)$ dominant components.

D. The ^{nat}Fe$(d,x)^{51}$Cr reaction

A more complex case is that of the activation cross sections of ^{51}Cr residual nucleus. The reported experimental activation cross sections are based on the measurements of 320 KeV γ-ray transition of ^{51}V [65,73–75], following the EC decay of the long-lived ^{51}Cr radionuclide ($T_{1/2} = 27.7$ d) [65,73,74]. However, since the ^{51}Cr nucleus is populated also by the EC decay of relatively short-lived ^{51}Mn ($T_{1/2} =$ 46.2 min) [65,73,75], as schematically presented in Fig. 18(a), the activation cross sections of ^{51}Cr that have been measured on the basis of this transition correspond to the reactions ^{54,56,57,58}Fe$(d,x)^{51}$Cr + ^{54,56,57,58}Fe$(d,x)^{51}$Mn. Therefore, in Fig. 18 are presented the main contributions to the activation of ^{51}Cr residual nucleus following the deuteron interactions with the ^{54,56,57,58}Fe isotopes, including the EC decay of

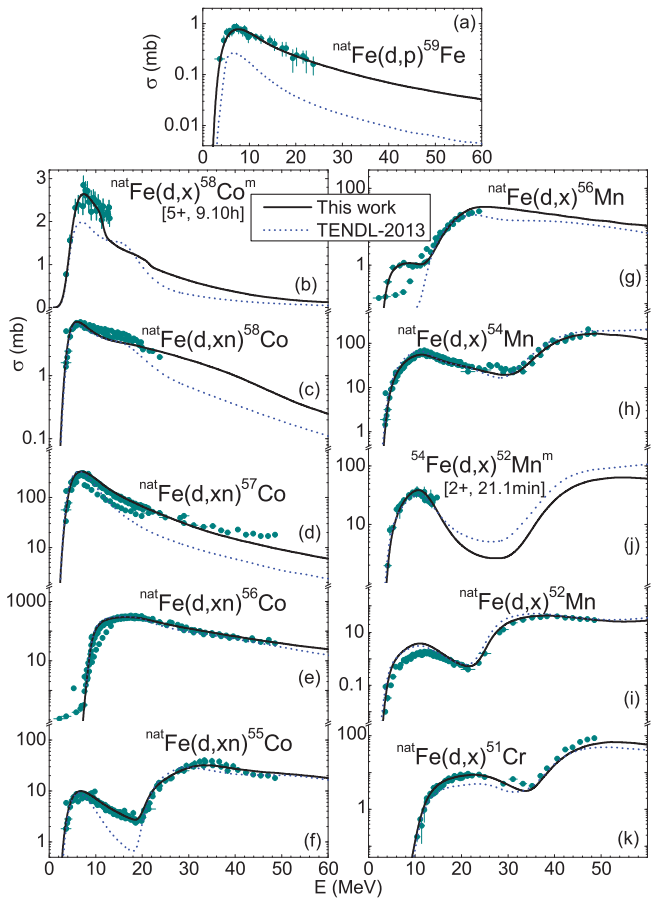

FIG. 19. (Color online) Comparison of previous [25–38] and present measurements (solid circles), present calculations (solid curves), and TENDL-2013 [19] predictions (dotted curves) of cross sections for deuteron interactions with ^{nat}Fe (see text).

the ^{51}Mn residual nucleus. A further distinct point of this reaction data analysis concerns the BF enhancement. It is present only in the case of the ^{54}Fe isotope, following the BU neutron and proton interactions with the target nucleus through the reactions ^{54}Fe$(n,\alpha)^{51}$Cr and ^{54}Fe$(p,\alpha)^{51}$Mn, respectively (Fig. 18). The corresponding cross sections have been added to the PE and CN contributions, corrected for the leakage of the initial deuteron flux toward direct processes, that are only present for the rest of ^{56,57,58}Fe isotopes.

E. Broad overview

Overall, the comparison of the calculated and evaluated TENDL-2013 [19] excitation functions shown in Fig. 19 has pointed out that the results of the present work are in better agreement with experimental data. Actually, the discrepancies between the experimental data and the corresponding TENDL-2013 predictions may underline the effects following the lack of BU enhancement contribution and the inappropriate treatment of the stripping and pick-up processes. Therefore, the use of coupled channels formalism for DR cross-section calculations could only make possible the description of excitation functions corresponding to one-particle emission that includes stripping, (d,p), (d,n), and pick-up, (d,t), (d,α), processes in addition to PE + CN mechanisms.

On the other hand, consideration of the deuteron breakup plays a key role for the reaction channels with a second and third emitted particle, in addition to the first one which could also be a BU nucleon. Thus, in order to obtain a complete description of either (d,xp) or (d,xn) reaction cross sections, it should be also taken into account that the neutrons/protons following the breakup proton/neutron emissions are absorbed in further interactions with the target nucleus. Finally, the deuteron activation cross sections represent the cumulative cross sections of either the (d,px) and (n,x) or the (d,nx) and (p,x) reactions with the same target nucleus.

V. CONCLUSIONS

The activation cross sections for production of ^{51}Cr, ^{52,54,56}Mn, ^{59}Fe, and ^{55,56,57,58}Co radioisotopes in deuteron-induced reactions on natural Fe were measured at deuteron energies up to 20 MeV. They are in good agreement with the previously reported experiments [25–38].

A major goal of the present work has been to evaluate the setting of an unitary analysis of the nuclear reaction mechanisms of the deuteron interactions with nuclei, namely the breakup, stripping, pick-up, preequilibrium, and statistical processes. It is required by the complexity of the deuteron interaction with nuclei, for which so far various weak approximations have been widely used.

A detailed theoretical treatment of each reaction mechanism contribution has thus been proved to be necessary to obtain a reliable understanding of the interaction process as well as to obtain accurate values of the calculated deuteron activation cross sections. Moreover, the comparisons of the experimental deuteron activation cross sections with both our model calculations and the corresponding TENDL-2013 evaluations support the detailed theoretical treatment of the deuteron interaction process. Firstly, the overall agreement between the measured data and model calculations validates the present theoretical approach of the deuteron interactions as well as each reaction mechanism that has been considered in this respect. On the other hand, the discrepancies between the measured data and corresponding TENDL-2013 evaluations have been explained as the result of overlooking the inelastic breakup enhancement, as well as of the inappropriate treatment of stripping and pick-up processes.

However, while the associated theoretical models for stripping, pick-up, PE, and CN are already settled, an increased attention should be paid to the breakup mechanism concerning its theoretical description including the inelastic component. Moreover, the improvement of the deuteron breakup description requires also complementary experimental studies of, e.g., (d,px) and (n,x) or of (d,nx) and (p,x) reaction cross sections for the same target nucleus, within corresponding incident-energy ranges [5]. Furthermore, the associated inclusive neutron and proton spectra measurements are required as well, since their analysis could make possible the distinction among various mechanism contributions. Thus, the only way to check and improve the breakup empirical parametrizations is to increase the related experimental databases.

ACKNOWLEDGMENTS

This work was partly supported by the Specific Grant Agreement GRT-168.01 of Fusion for Energy (F4E), Barcelona, and by a grant of the Romanian National Authority for Scientific Research, CNCS-UEFISCDI, Project No. PN-II-ID-PCE-2011-3-0450.

[1] M. Avrigeanu, W. von Oertzen, R. A. Forrest, A. C. Obreja, F. L. Roman, and V. Avrigeanu, Fusion Eng. Design **84**, 418 (2009).

[2] P. Bém, E. Šimečková, M. Honusek, U. Fischer, S. P. Simakov, R. A. Forrest, M. Avrigeanu, A. C. Obreja, F. L. Roman, and V. Avrigeanu, Phys. Rev. C **79**, 044610 (2009).

[3] M. Avrigeanu and A. M. Moro, Phys. Rev. C **82**, 037601 (2010).

[4] E. Šimečková, P. Bém, M. Honusek,M. Štefánik, U. Fischer, S. P. Simakov, R. A. Forrest, A. J. Koning, J.-C. Sublet, M. Avrigeanu, F. L. Roman, and V. Avrigeanu, Phys. Rev. C **84**, 014605 (2011).

[5] M. Avrigeanu, V. Avrigeanu, and A. J. Koning, Phys. Rev. C **85**, 034603 (2012).

[6] M. Avrigeanu, V. Avrigeanu, P. Bém, U. Fischer, M. Honusek, A. J. Koning, J. Mrázek, E. Šimečková, M. Štefánik, and L. Závorka, Phys. Rev. C **88**, 014612 (2013).

[7] International Thermonuclear Experimental Reactor (ITER), http://www.iter.org/proj.

[8] International Fusion Material Irradiation Facility (IFMIF), http://www.ifmif.org/b/.

[9] Neutron For Science (NFS) project, Systéme de Production d'Ions Radioactifs en Ligne, generation 2 (SPIRAL-2), http://pro.ganil-spiral2.eu/spiral2/instrumentation/nfs.

[10] Fusion Evaluated Nuclear Data Library (FENDL) 3.0, http://www-nds.iaea.org/fendl3/.

[11] M. Avrigeanu and V. Avrigeanu, EPJ Web Conf. **2**, 01004 (2010).

[12] M. Avrigeanu and V. Avrigeanu, J. Phys.: Conf. Ser. **205**, 012014 (2010).

[13] E. Šimečková, P. Bém, M. Götz, M. Honusek, J. Mrázek, J. Novák, M. Štefánik, L. Závorka, M. Avrigeanu, and V. Avrigeanu, EPJ Web Conf. **8**, 07002 (2010).

[14] M. Avrigeanu and V. Avrigeanu, J. Korean Phys. Soc. **59**, 903 (2011).

[15] E. Šimečková, P. Bém, M. Honusek, L. Závorka, U. Fischer, S. P. Simakov, R. A. Forrest, M. Avrigeanu, V. Avrigeanu, and F. L. Roman, J. Korean Phys. Soc. **59**, 1928 (2011).

[16] M. Avrigeanu and V. Avrigeanu, EPJ Web Conf. **21**, 07003 (2012).

[17] I. J. Thompson, Comput. Phys. Rep. **7**, 167 (1988).

[18] A. J. Koning, S. Hilaire, and M. C. Duijvestijn, v. TALYS-1.4, 2011, http://www.talys.eu.

[19] A. J. Koning and D. Rochman, TENDL-2013: TALYS-Based Evaluated Nuclear Data Library, 2013, http://www.talys.eu/tendl-2013/.

[20] L. Závorka, E. Šimečková, M. Honusek, and K. Katovsky, J. Korean Phys. Soc. **59**, 1961 (2011).

[21] M. Avrigeanu and V. Avrigeanu, in *Proceedings of the International Conference on Nuclear Data for Science and Technology, New York, March* 2013 [Nucl. Data Sheets (to be published)].

[22] M. Avrigeanu and V. Avrigeanu, in Proceedings of the XX International School on Nuclear Physics, Neutron Physics and Applications, Varna, September 2013 [J. Phys.: Conf. Ser. (to be published)].

[23] J. F. Ziegler, J. P. Biersack, and M. D. Ziegler, SRIM–The Stopping and Range of Ions in Matter, SRIM code, http://www.srim.org.

[24] S. Y. F. Chu, L. P. Ekström, and R. B. Firestone, The Lund/LBNL Nuclear Data, Search Version 2.0, February 1999, http://nucleardata.nuclear.lu.se/toi/.

[25] B. Kiraly, S. Takacs, F. Ditroi, F. Tarkanyi, and A. Hermanne, Nucl. Instrum. Methods Phys. Res. B **267**, 15 (2009).

[26] M. U. Khandaker, H. Haba, J. Kanaya, and N. Otuka, Nucl. Instrum. Methods Phys. Res. B **316**, 33 (2013).

[27] Z. Wenrong, L. Hanlin, Y. Weixiang, and C. Jianto, Chin. J. Nucl. Phys. **17**, 163 (1995); EXFOR Data Entry No. S0044 dated 1999-07-26, http://www-nds.iaea.org/exfor.

[28] S. Sudar and S. M. Qaim, Phys. Rev. C **50**, 2408 (1994).

[29] S. Sudar and S. M. Qaim, Phys. Rev. C **53**, 2885 (1996).

[30] S. Takacs, F. Tarkanyi, M. Sonck, A. Hermanne, and S. Sudar, in Proceedings of the Conference on Applications of Accelerators in Research and Industry, Denton, TX, 1996 (unpublished), p. 659; EXFOR Data Entry No. D4044 dated 1996-07-13, http://www-nds.iaea.org/exfor.

[31] A. Hermanne, M. Sonck, S. Takacs, and F. Tarkanyi, Nucl. Instrum. Methods Phys. Res. B **161-163**, 178 (2000).

[32] K. Ochiai, M. Nakao, N. Kubota, S. Sato, M. Yamauchi, N. H. Ishioka, T. Nishitani, and C. Konno, in *Proceedings of the International Conference on Nuclear Data for Science and Technology, Nice, 2007*, edited by O. Bersillon, F. Gunsing, E. Bauge, R. Jacqmin, and S. Leray (EDP Sciences, Paris, 2008), p. 1011.

[33] T. Zhenlan, Z. Fuying, Q. Huiyuan, and W. Gongoing, At. Energy Sci. Technol. **18**, 506 (1984); EXFOR Data Entry No. S0015 dated 1985-05-17, http://www-nds.iaea.org/exfor.

[34] P. Jung, in *Proceedings of the International Conference on Nuclear Data for Science and Technology, Juelich, 1991*, edited by S. M. Qaim (Springer, Berlin Heidelberg, 1992), p. 352.

[35] S. Takacs, F. Szelecsenyi, F. Tarkanyi, M. Sonck, A. Hermanne, Yu. Shubin, A. Dityuk, M. G. Mustafa, and Zhuang Youxiang, Nucl. Instrum. Methods Phys. Res. B **174**, 235 (2001).

[36] M. Nakao, J. Hon, K. Ochiai, N. Kubota, S. Sato, M. Yamauchi, N. S. Ishioka, and T. Nishitani, Nucl. Instrum. Methods Phys. Res. A **562**, 785 (2006).

[37] M. R. Zaman and S. M. Qaim, Radiochim. Acta **75**, 59 (1996).

[38] P. P. Coetzee and M. Peisach, Radiochim. Acta **17**, 1 (1972).

[39] F. James and M. Foos, Comput. Phys. Commun. **10**, 343 (1975).

[40] R. C. Brown, A. A. Debenham, J. A. R. Griffith, O. Karban, D. C. Kocher, and S. Roman, Nucl. Phys. A **208**, 589 (1973); R. P. Goddard and W. Haeberli, *ibid.* **316**, 116 (1979); S. A. Hjorth, E. K. Lin, and A. Johnson, *ibid.* **116**, 1 (1968); E. Newman, L. C. Becker, B. M. Preedom, and J. C. Hiebert, *ibid.* **100**, 225 (1967); F. Hinterberger, G. Mairle, U. Schmidt-Rohr, G. J. Wagner, and P. Turek, *ibid.* **111**, 265 (1968); R. De Leo *et al.*, Phys. Rev. C **53**, 2718 (1996); S. I. Al-Quraishi, C. E. Brient, S. M. Grimes, T. N. Massey, J. Oldendick, and R. Wheeler, *ibid.* **62**, 044616 (2000); R. Roche, Nguyen Van Sen, G. Perrin, J. C. Gondrand, A. Fiore, and H. Muller, Nucl. Phys. A **220**, 381 (1974); K. C. McLean, S. M. Dalgliesh, S. S. Ipson, and G. Brown, *ibid.* **191**, 417 (1972).

[41] C. M. Perey and F. G. Perey, Phys. Rev. **132**, 755 (1963).

[42] J. M. Lohr and W. Haeberli, Nucl. Phys. A **232**, 381 (1974).

[43] W. W. Daehnick, J. D. Childs, and Z. Vrcelj, Phys. Rev. C **21**, 2253 (1980).
[44] J. Bojowald, H. Machner, H. Nann, W. Oelert, M. Rogge, and P. Turek, Phys. Rev. C **38**, 1153 (1988).
[45] H. An and C. Cai, Phys. Rev. C **73**, 054605 (2006).
[46] C. Kalbach Walker, Triangle University Nuclear Laboratory Progress Report No. XLII 2002–2003 (unpublished), pp. 82–83; www.tunl.duke.edu/publications/tunlprogress/2003/.
[47] C. Kalbach Walker, IAEA Report to the 2nd Research Coordination Meeting of the Fusion Evaluated Nuclear Data Library FENDL 3.0, 23–26 March 2010 (unpublished), and references therein; http://www-nds.iaea.org/fendl3/vardocs.html.
[48] J. Pampus, J. Bisplinghoff, J. Ernst, T. Mayer-Kuckuk, J. Rama Rao, G. Baur, F. Rosel, and D. Trautmann, Nucl. Phys. A **311**, 141 (1978).
[49] J. R. Wu, C. C. Chang, and H. D. Holmgren, Phys. Rev. C **19**, 370 (1979).
[50] N. Matsuoka, M. Kondo, A. Shimizu, T. Saito, S. Nagamachi, H. Sakaguchi, A. Goto, and F. Ohtani, Nucl. Phys. A **345**, 1 (1980).
[51] J. Kleinfeller, J. Bisplinghoff, J. Ernst, T. Mayer-Kuckuk, G. Baur, B. Hoffmann, R. Shyam, F. Rosel, and D. Trautmann, Nucl. Phys. A **370**, 205 (1981).
[52] M. G. Mustafa, T. Tamura, and T. Udagawa, Phys. Rev. C **35**, 2077 (1987).
[53] Experimental Nuclear Reaction Data (EXFOR), http://www-nds.iaea.org/exfor.
[54] M. Avrigeanu, W. von Oertzen, U. Fischer, and V. Avrigeanu, Nucl. Phys. A **759**, 327 (2005).
[55] M. Kawai, M. Kamimura, and K. Takesako, Prog. Theor. Phys. Suppl. **89**, 118 (1986).
[56] P. Guazzoni, L. Zetta, A. Covello, A. Gargano, B. F. Bayman, T. Faestermann, G. Graw, R. Hertenberger, H.-F. Wirth, and M. Jaskola, Phys. Rev. C **83**, 044614 (2011).
[57] R. M. DelVecchio, Phys. Rev. C **7**, 677 (1973).
[58] H. Junde, Nucl. Data Sheets **109**, 787 (2008).
[59] M. R. Bhat, Nucl. Data Sheets **85**, 415 (1998).
[60] C. M. Baglin, Nucl. Data Sheets **95**, 215 (2002).
[61] H. Junde, Nucl. Data Sheets **110**, 2689 (2009).
[62] H. Junde, H. Su, and M. A. Chunhui, Nucl. Data Sheets **108**, 773 (2007).
[63] H. Junde and H. Su, Nucl. Data Sheets **107**, 1393 (2006).
[64] H. Junde, H. Su, and Y. Dong, Nucl. Data Sheets **112**, 1513 (2011).
[65] Evaluated Nuclear Structure Data File (ENSDF), http://www.nndc.bnl.gov/ensdf/.
[66] M. Mahgoub *et al.*, Eur. Phys. J. A **40**, 35 (2009).
[67] M. Hagen, U. Janetzki, and K. H. Maier, Nucl. Phys. A **157**, 177 (1970).
[68] P. Gaillard, J- Y. Grossiord, and A. Guichard, Phys. Rev. C **7**, 1147 (1973).
[69] M. R. Zaman, S. Spellberg, and S. M. Qaim, Radiochim. Acta **91**, 105 (2003).
[70] A. J. Koning and J. P. Delaroche, Nucl. Phys. A **713**, 231 (2003).
[71] V. Avrigeanu, P. E. Hodgson, and M. Avrigeanu, Phys. Rev. C **49**, 2136 (1994).
[72] F. D. Becchetti, Jr. and G. W. Greenlees, Annual Report, J. H. Wiliams Laboratory, University of Minesota, 1969 (unpublished).
[73] Huang Xiaolong, Nucl. Data Sheets **107**, 2131 (2006).
[74] P. Yalcin and Y. Kurucu, Appl. Radiat. Isot. **62**, 63 (2005); R. G. Helmer and C. van der Leun, Nucl. Instrum. Methods Phys. Res. A **450**, 35 (2000).
[75] J. C. Ferrer, J. Rapaport, and S. Raman, Z. Phys. **265**, 365 (1973); K. M. Glibert and H. T. Easterday, Nucl. Phys. A **86**, 279 (1966).